

Expansion behavior of concrete containing different steel slag aggregate sizes under heat curing

Chun-Ya Shu^a and Wen-Ten Kuo^{*}

Department of Civil Engineering, National Kaohsiung University of Applied Sciences,
No. 415, Chien-Kung Rd., Sanmin District, Kaohsiung 80778, Taiwan, R.O.C.

(Received July 22, 2015, Revised August 31, 2015, Accepted September 1, 2015)

Abstract. This study investigated particle expansion in basic oxygen furnace slag (BOF) and desulfurization slag (DSS) after heat curing by using the volume method. Concrete hydration was accelerated by heat curing. The compressive strength, ultrasonic pulse velocity, and resistivity of the concrete were analyzed. Maximum expansion occurred in the BOF and DSS samples containing 0.30-0.60 mm and 0.60-1.18 mm particles, respectively. Deterioration was more severe in the BOF samples. In the slag aggregates for the complete replacement of fine aggregate, severe fractures occurred in both the BOF and DSS samples. Scanning electron microscopy revealed excess CH after curing, which caused peripheral hydration products to become extruded, resulting in fracture.

Keywords: basic oxygen furnace slag (BOF); desulfurization slag (DSS); aggregate particle size; heat curing; expansion effect

1. Introduction

The byproduct of steel slag from steelmaking processes is frequently used as a concrete mixing material. However, the unstable process and quality of the material typically cause volumetric expansion. Many studies investigating the use of steel slag as an aggregate in concrete have described its advantageous properties (Li *et al.* 2009, Wang 2010, Etxeberria *et al.* 2010). The physical properties of steel slag render it highly suitable for use in construction because it enhances the characteristics of end products (Sorlini *et al.* 2012, Sofilic *et al.* 2010, Wu *et al.* 2007). In addition, crushed air-cooled blast furnace slag used in high-strength concrete possesses superior mechanical properties compared with natural limestone concrete (Wang *et al.* 2012). Therefore, steel slag has been considered comparable to common stone materials employed in civil engineering applications (Yildirim and Prezzi 2009, Huang *et al.* 2007, Ivanka 2011). The annual output of basic oxygen furnace (BOF) slag and desulfurization slag (DSS) as a byproduct of steel making in Taiwan (Lun *et al.* 2008) is approximately 1.5 million megatons, accounting for approximately 25 wt% of byproducts. After undergoing treatment, BOF and DSS can be used to

*Corresponding author, Professor, E-mail: wtkuo@cc.kuas.edu.tw

^aPh.D. Candidate, E-mail: chunya@hcv.s.kh.edu.tw

replace natural aggregates (Siddique 2009, Shen *et al.* 2009a, b) as a mixing material for road backfill and foundation ground backfill (US federal environment protection agency 2010, Suer *et al.* 2009, Ahmedzade and Sengoz 2009). Using these aggregates can reduce waste landfill and excessive natural resource consumption, and enhance the efficiency of waste material reutilization (Naganathan *et al.* 2012, Naganathan *et al.* 2010, Waligora *et al.* 2010). However, the presence of free-CaO (f-CaO) and free-MgO (f-MgO) in engineering materials can produce notable long-term volumetric swelling caused by the volumetric expansion resulting from the spontaneous hydration of these compounds at room temperature (Ortega-Lopez *et al.* 2014, Auriol 2004). This problem can be addressed through appropriate steel slag aging and quality control, particularly appropriate testing to ensure its suitability for use in construction (Wang *et al.* 2010, Ameri and Ali 2012). Hydration of f-CaO and f-MgO occurs slowly at a normal temperature (Li and Li 2005). Kuo (Kuo and Shu 2014, Kuo *et al.* 2014, Kuo and Shu 2015) applied a high-temperature rapid catalytic technology to accelerate the hydration reaction for the rapid forecasting of volumetric instability in steel. Wang (Wang 2014) proposed that the stability of slag can be confirmed through the autoclave expansion of a slag mortar bar.

The particle size and gradation of aggregate are related to volumetric expansion (Multon *et al.* 2008, Lukschova *et al.* 2009). Some previous studies have indicated that exceedingly small particles in active aggregates can effectively reduce the expansion behavior (Poyet *et al.* 2007, Cyr *et al.* 2009). Cyr *et al.* (Cyr *et al.* 2009) examined various types of finely ground reactive aggregate and found that all of them were effective in reducing expansion. Furthermore, powder from reactive aggregates such as pozzolans, with particle sizes up to approximately 100 μm , has been developed to counteract the effect of alkali–silica reaction (ASR). Particles in aggregates with alkali reactivity are subject to the pessimum size effect (Lin *et al.* 2013, Multon *et al.* 2010), meaning that active particle sizes within a specific range produce the maximum expansion. To eliminate the influence of ASR, the present study controlled the cement alkali content to be less than 0.6% $\text{Na}_2\text{O}_{\text{eq}}$, thereby avoiding the influence of aggregates in the course of the reaction with alkali.

In this study, BOF and DSS with various particle sizes were used to replace natural fine aggregate. Through determination of the expansion deterioration difference between particle sizes after heat curing, particle sizes that may cause deterioration can be discarded in advance to render these materials more suitable for engineering applications.

2. Materials and methods

2.1 Materials

The BOF and DSS used in this study were derived from a local steelmaking factory in Taiwan. Because the particle sizes that cause deterioration had to be determined, separate screenings were implemented according to the particle size, and natural fine aggregate was replaced by particles of a specific size. The material was identified as safe according to the toxicity characteristic leaching procedure. Tables 1 and 2 show the results of chemical analysis and physical characteristics. The BOF and DSS contain SiO_2 , Fe_2O_3 , and CaO, which account for approximately 90% of the chemical composition, with the free lime content being 3.09% and 2.08%; lime is a crucial source of expansion (Chaurand *et al.* 2007). Natural sand conforming to ASTM C33 was used. The cement was tested according to ASTM C114 and the properties of cement conformed to ASTM

C150.

2.2 Mix proportions

The volumetric method was used according to ASTM C1293, and the volumes of particles of various sizes were fixed to calculate the mix proportion. All the materials were processed using separating screens, which were classified according to the particle size: 2.36-4.75 mm (F1);

Table 1 Physical characteristics of cement, BOF and DSS (%)

Material	Al ₂ O ₃	SiO ₂	Fe ₂ O ₃	CaO	MgO	K ₂ O	SO ₃	Na ₂ O	TiO ₂	Na ₂ O _{eq}	f- CaO
Cement	4.96	20.22	2.83	64.51	2.33	--	--	--	--	0.50	--
BOF	2.57	10.60	28.32	46.38	5.28	0.05	0.35	0.19	0.46	--	3.09
DSS	2.35	18.51	16.10	55.41	1.76	0.03	2.21	0.10	0.15	--	2.58

Table 2 Chemical characteristics of slag and natural sand.

particle size (mm)	BOF		DSS		natural sand		
	Specific	Absorption (%)	Specific	Absorption	Specific	Absorption	
2.36~4.75 (F1)		3.40	2.7	2.48	6.2	2.64	1.6
1.18~2.36 (F2)		3.23	3.1	2.38	8.7	2.63	1.8
0.60~1.18 (F3)		3.21	4.8	2.16	10.7	2.61	2.4
0.30~0.60 (F4)		2.96	7.1	1.95	15.2	2.60	2.7
0.15~0.30 (F5)		2.75	10.2	1.89	20.7	2.58	3.1

Table 3 Mixture proportions of steel slag concrete (Unit: kg/m³)

Item	Cement	Water	Aggregate							
			12.5~19	9.5~12.5	4.75~9.5	F1	F2	F3	F4	F5
particle size	--	--	12.5~19	9.5~12.5	4.75~9.5	F1	F2	F3	F4	F5
Mass (%)	--	--	33	33	33	10	25	25	25	15
Ref.	420	189	346	346	346	75	188	188	188	113
BOF	F1	420	189	346	346	346	97♦	188	188	113
	F2	420	189	346	346	346	75	231♦	188	113
	F3	420	189	346	346	346	75	188	230♦	113
	F4	420	189	346	346	346	75	188	188	212♦
	F5	420	189	346	346	346	75	188	188	118♦
	FA	420	189	346	346	346	97♦	231♦	230♦	212♦
DSS	F1	420	189	346	346	346	71♦	188	188	113
	F2	420	189	346	346	346	75	170♦	188	113
	F3	420	189	346	346	346	75	188	154♦	113
	F4	420	189	346	346	346	75	188	188	140♦
	F5	420	189	346	346	346	75	188	188	81♦
	FA	420	189	346	346	346	71♦	170♦	154♦	140♦

Note 1. Among the mixture number, ♦ is steel slag replaced natural aggregates volume completely.

Note 2. F1 : 2.36~4.75 mm, F2 : 1.18~2.36 mm, F3 : 0.60~1.18 mm, F4 : 0.30~0.60 mm, F5 : 0.15~0.30 mm, FA : all natural aggregates were replaced with slag aggregates.

1.18-2.36 mm (F2); 0.6-1.18 mm (F3); 0.3-0.6 mm (F4); and 0.15-0.3 mm (F5). All natural aggregates were replaced with slag aggregates (FA), and natural fine aggregate was replaced with BOF and DSS with corresponding particle sizes according to volume ratio. The natural aggregates containing particles of other sizes were retained to investigate the mutual expansion behavior. Table 3 shows the mix proportion of various groups of concrete: the cement content was 420 kg/m³, the water-cement ratio was 0.45, and the volume ratio of coarse-to-fine aggregates was 1:0.73.

2.3 Methods

The heat curing method employed in this study was autoclave expansion, which conforms to ASTM C151, and “100°C cure” was applied to investigate the expansion behavior. The term “100°C cure” means that samples were placed in a curing tank with a controlled temperature, which was set to 100°C, and a relative humidity of 100%. The samples were removed every other day to measure the change in length and were then placed back into the water tank. The test period was 14 days. The compressive strength, ultrasonic pulse velocity, and surface resistance of the samples were tested to observe the mechanical behavior and durability. Scanning electron microscopy (SEM) and X-ray diffraction (XRD) were implemented in examining the sample on Days 3 and 14 of curing (or on the day of fracture) to observe the hydration and changes in the chemical composition.

3. Results and discussion

3.1 Autoclave expansion

Each natural fine aggregate was replaced with BOF and DSS with the same particle size for autoclave expansion (Fig. 1). Shrinkage of all alternate material particles was greater than that of

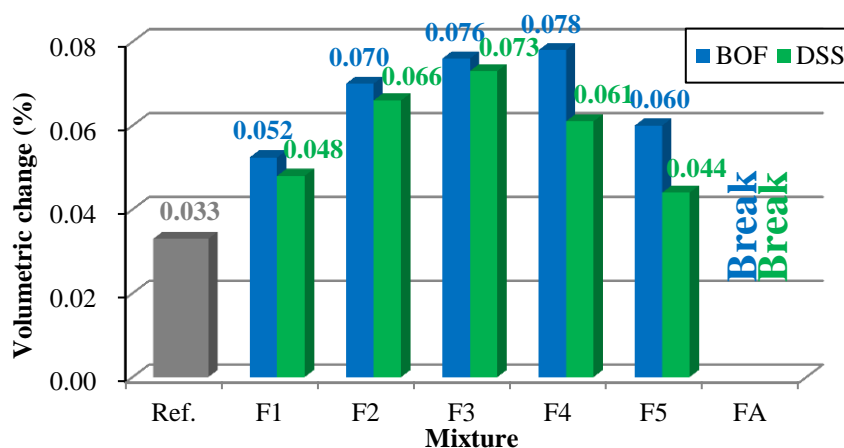


Fig. 1 The BOF and DSS slag volumetric change of the autoclave expansion (Slag corresponding to the same particle size of natural fine aggregate is replaced)



Fig. 2 The BOF concrete of the autoclave expansion images



Fig. 3 The DSS concrete of the autoclave expansion images

the control (Ref.), and the expansion values of BOF were larger than those of DSS. The maximum particle size 2.36-4.75 mm (F1) and minimum particle size 0.15-0.30 mm (F5) produced a negligible response, and the rate of change in 1.18-2.36 mm (F2), 0.60-1.18 mm (F3), and 0.30-0.60 mm (F4) samples was 84%-136% higher than that of the control group. This is similar to the ASR particle size expansion findings reported by Multon (Multon *et al.* 2010), who measured no expansion in mortars containing small particles ($<80 \mu\text{m}$), whereas the coarse particles (0.63-1.25 mm) produced the largest expansions. The expansion of Taiwan's furnace slag was not caused by the ASR, but by the embedded f-CaO and f-MgO (Lin 2006, Yu 2011). Chemical analysis indicated that the f-CaO content in the BOF was 3.09%, which was higher than that in the DSS (2.58%), implying that the expansion values correlated with the f-CaO content; in other words, the higher the f-CaO content is, the higher the expansion values. Regarding the FA for the complete replacement of fine aggregate particles, the two materials exhibited severe fracture and fragments spallation (Figs. 2 and 3). However, the failure modes differed, and the BOF failure was extensible. The end of the sample was not crushed completely (part of a blocky structure remained), whereas the end of DSS was crushed completely. Figs. 2 and 3 show a few points of burst and white powdered crystals on the F1, F2, and F3 surfaces, and the 1.18-2.36 mm (F2) surface reaction is more apparent. In general, the larger the replacement particle size is, the more apparent the surface fracture. However, F1 accounted for only 10 wt% of the fine aggregate, and F2, F3, and F4 accounted for 25 wt%; thus, the F2 surface fracture effect was greater than that for

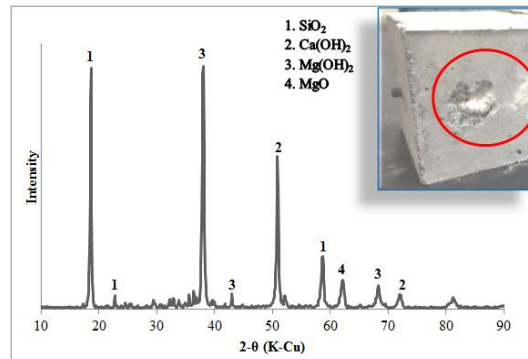


Fig. 4 XRD of white crystalline at rupture points

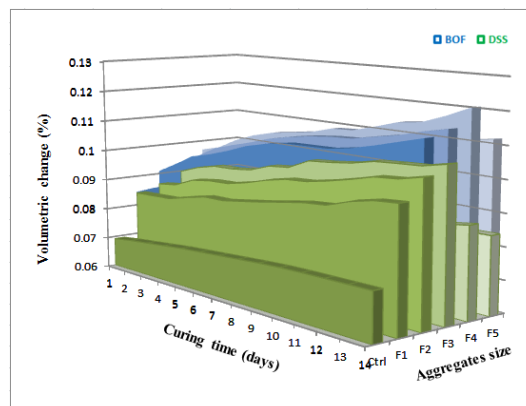


Fig. 5 Replace single particle size expansion distribution area

F1. The white crystals were collected for XRD analysis, which revealed the crystals to be $\text{Ca}(\text{OH})_2$ and $\text{Mg}(\text{OH})_2$ (Fig. 4), validating the aforementioned test result.

3.2 100°C Curing

Various sample groups were placed in the 100°C constant-temperature tank for heat curing. Fig. 5 shows the expansion distribution area over the 14 days. The expansion values increased with the curing age, the BOF volumetric change was apparently greater than that in the DSS, and the main particle sizes for the maximum expansion effect were 1.18-2.36 mm (F2), 0.60-1.18 mm (F3), and 0.30-0.60 mm (F4), although the effect was more apparent for the 0.60-1.18 mm (F3) and 0.30-0.60 mm (F4) samples, which is similar to the autoclave expansion results. Regarding the expansion values when various materials were used to replace particles of a single size, various mix proportions were cured at 100°C, and the expansion values were initially higher than those in the control group. The expansion value of the control group plateaued as the curing age increased, precluding the possibility that expansion resulted from the natural aggregate. Fig. 6 shows the expansion values for BOF used to replace fine aggregate of a single particle size. According to Kamile (Kamile 2006), in the long run, the expansion rate of cement mortar containing fine particles exceeds the expansion value of coarse particles, and our test results show that the

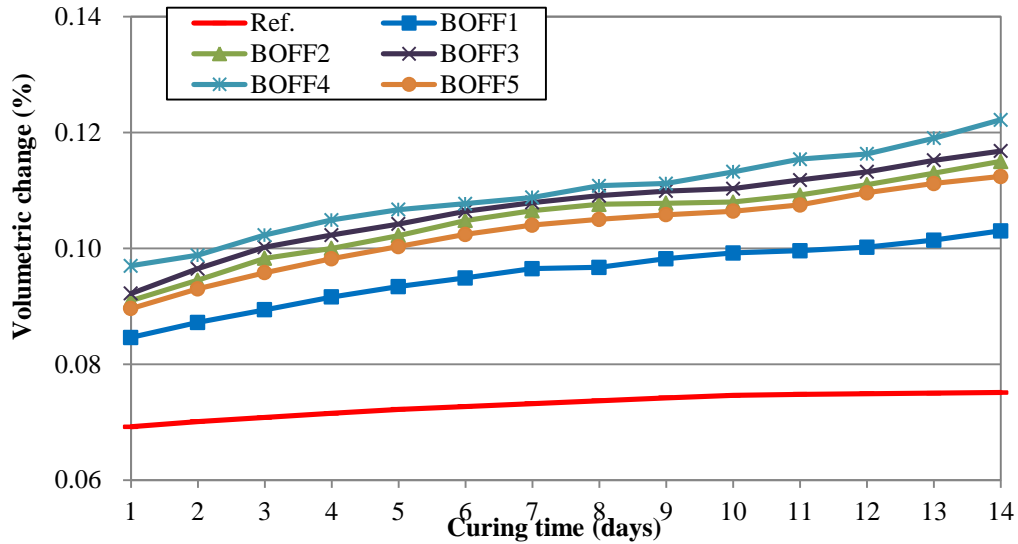


Fig. 6 BOF replaced single particle size volumetric change and curing time relationship (100°C)

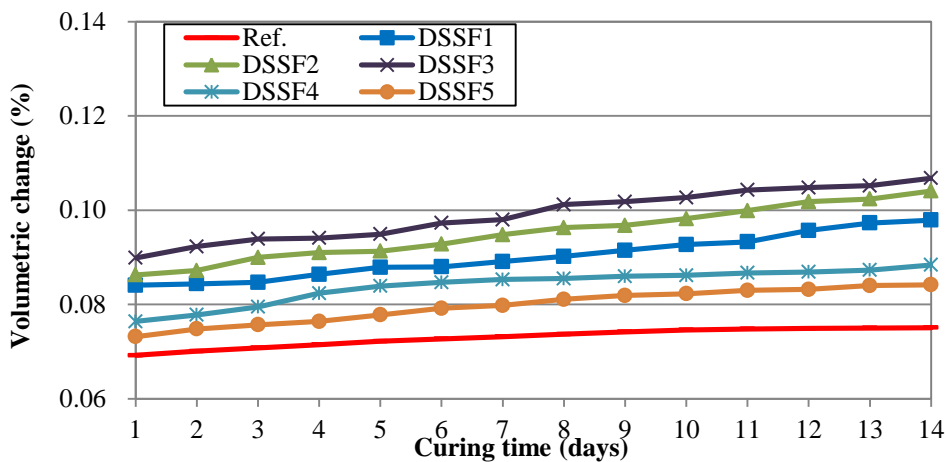


Fig. 7 DSS replaced single particle size volumetric change and curing time relationship (100°C)

particles sizes can be ordered as follows according to the expansion values: 0.30-0.60 mm (F4) > 0.60-1.18 mm (F3) > 1.18-2.36 mm (F2) > 0.15-0.30 mm (F5) > 2.36-4.75 mm (F1). According to the expansion values from the Days 1 to 14, the expansion rate of the small particle size (F4) was increased by approximately 5% compared with the large particle size (F1). Fig. 7 shows the expansion values for DSS used to replace fine aggregate of a single particle size; the results corroborate those of the BOF experiment. The order of the particle sizes according to expansion values is 0.60-1.18 mm (F3) > 1.18-2.36 mm (F2) > 2.36-4.75 mm (F1) > 0.30-0.60 mm (F4) > 0.15-0.30 mm (F5). The particle sizes that underwent the largest change were F4 and F1, which should have resulted in the maximum expansion; however, no obvious reaction was observed. This is because of the high fineness, particularly because high-temperature curing typically accelerates

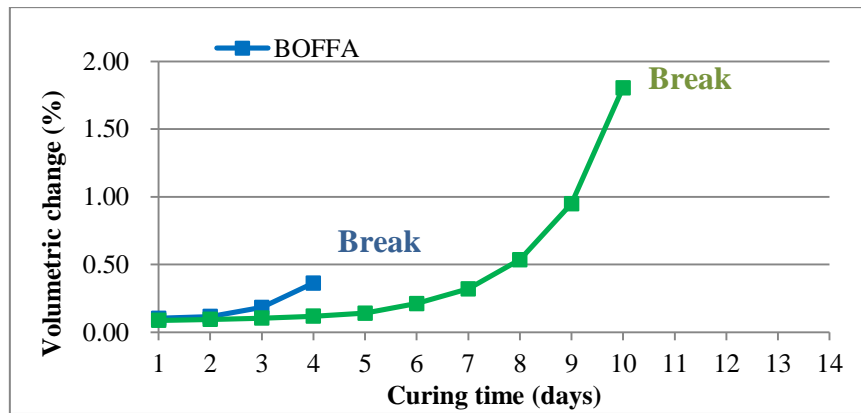


Fig. 8 The heat curing results at various ages of complete replacement for fine aggregate particle size (100°C)

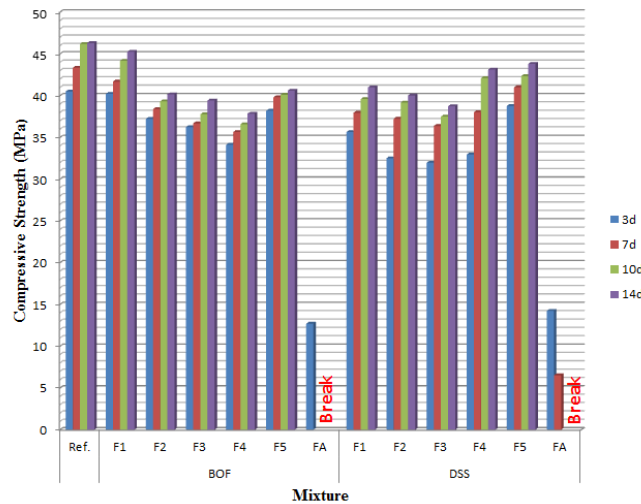


Fig. 9 Compressive strength and curing time relationship (100°C)

the reaction of SO_3 and Al_2O_3 (Kelham 2006). According to the composition, the Al_2O_3 content in the DSS was 1.73%, which differs slightly from that in the BOF, and the SO_3 content was 4.21%, which was considerably higher than that in the BOF (0.35%). Fig. 7 shows that the expansion ratio of F4 increased rapidly before Day 4, the expansion ratio plateaued after Day 5, and the expansion of F1 increased obviously after Day 3. The solubility of SO_3 is related to the particle size, and the product of the reaction between the active material on the fine particle surface and the cement hydration product was wrapped in the aggregate surface, effectively inhibiting SO_3 leaching and ettringite formation (Bi *et al.* 2004, Yin and Xie 2007). Fig. 8 shows the heat curing results at various ages for complete replacement of the fine aggregate particles. Because the natural fine aggregate was replaced, the expansion values were apparently higher than those of the various mix proportions for replacing particles of a single size, and the sample fractures on Days 5 and 11 could not be measured. The expansion value of BOF FA reached 0.1036% on Day 1 of curing, and approached the swelling value of the group for replacing particles of a single size on Days 4 and 5.

Table 4 Ultrasonic pulse velocity and curing time relationship (100°C)

Curing time (days)		Ultrasonic Pulse Velocity (m/s)			
		3	7	10	14
	Ref.	4556	4630	4662	4662
BOF	F1	4480	4522	4531	4586
	F2	4354	4412	4473	4480
	F3	4330	4348	4391	4425
	F4	4309	4334	4337	4381
	F5	4370	4448	4505	4505
	FA	2375	Break	Break	Break
DSS	F1	4337	4389	4393	4490
	F2	4264	4344	4373	4465
	F3	4242	4329	4357	4389
	F4	4292	4357	4408	4525
	F5	4467	4486	4565	4591
	FA	2531	1657	Break	Break

The expansion became unstable after Day 2, reaching 0.1834% on Day 3. The expansion rate peaked at 97.8% on Day 4. The DSSFA expansion rate increased with the curing age, and the expansion ratio increased by 50%-90% daily until fracture on Day 10.

3.3 Compressive strength, ultrasonic pulse velocity, and resistivity

Fig. 9 shows the compressive strength of the mix proportions cured at 100°C. The results show that the compressive strength of all mix proportions at various ages was lower than that of the control group. The FA mix proportion for complete replacement of the aggregate fractured during the curing period; consequently, the compressive strength was reduced. The compressive strength of the other mix proportions increased with the curing time. In the replacement of fine aggregate particles of a single size with BOF, the 0.30-0.60 mm (F4) sample achieved the minimum compressive strength; the ratio of the compressive strength at various ages to that of the control group was approximately 79%-84%. The 2.36-4.75 mm (F1) sample achieved the most favorable result; the ratio of the compressive strength at various ages to the strength of the control group was 96%-99%. In the replacement of fine aggregate particles of a single size with DSS, 0.60-1.18 mm (F3) achieved the minimum compressive strength, followed by 1.18-2.36 mm (F2) and 2.36-4.75 mm (F1), and the 0.15-0.30 mm (F5) sample achieved the maximum strength; the ratio of the compressive strength at various ages to that of the control group was approximately 92%-96%. Table 4 shows the ultrasonic pulse velocity of various mix proportions cured at 100°C. The strength of all mix proportions at various ages was lower than that of the control group. In the replacement of fine aggregate particles of a single size with BOF, the 0.30-0.60 mm (F4) sample had the minimum strength and the 2.36-4.75 mm (F1) sample had the maximum strength. The ratio of the strength of these samples to that of the control group at various ages was 93%-95% and 97%-98%. The difference between the ultrasonic pulse velocities was 150-200 m/s. In the replacement of fine aggregate particles of a single size with DSS, the 0.60-1.18 mm (F3) sample had the minimum strength and the 0.15-0.30 mm (F5) sample had the maximum strength; the pulse velocity ratios were 93%-94% and 97%-98%, respectively. The strength of the mix

Table 5 Resistivity values and curing time relationship (100°C)

		Resistivity Values (kΩ-cm)			
Curing time (days)		3	7	10	14
	Ref.	9.0	10.1	11.3	12.0
BOF	F1	8.7	9.7	11.0	11.8
	F2	8.4	9.3	10.8	11.6
	F3	8.0	9.3	10.2	10.9
	F4	8.0	8.8	10.0	10.2
	F5	8.7	9.5	11.0	11.6
	FA	5.9	Break	Break	Break
DSS	F1	8.4	8.9	10.1	10.9
	F2	7.8	8.9	9.9	10.6
	F3	7.8	8.6	9.9	10.4
	F4	8.1	9.2	10.4	11.3
	F5	8.8	9.8	10.9	11.7
	FA	7.3	4.3	Break	Break

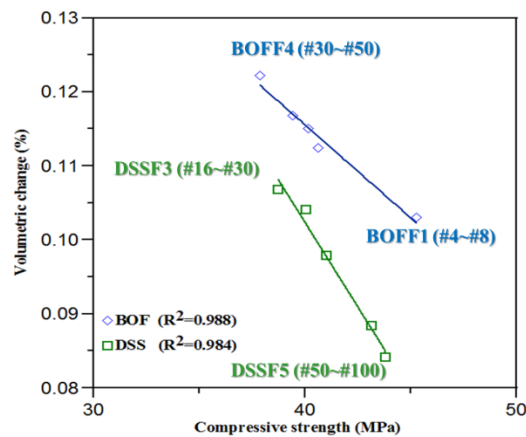


Fig. 10 Slag replaced single particle size volumetric change and compressive strength relationship (100°C, 14 day)

proportion for complete replacement of the aggregate was the minimum compared with that of the mix proportions for replacement of particles of a single size; the pulse velocity of the BOF FA was only 2375 m/s on Day 3, and the pulse velocity of the DSS FA was only 2531 m/s on Day 3 and 1657 m/s on Day 7, after which the sample fractured. Table 5 shows the resistivity of various mix proportions. In the replacement of particles of a single size with BOF, the 0.30-0.60 mm (F4) and 2.36-4.75 mm (F1) samples achieved the minimum and maximum resistivity, respectively, and the ratios of the compressive strength at various ages to that of the control group were 85%-89% and 96%-98%, respectively. In the replacement of fine aggregate particles of a single size with DSS, the 0.60-1.18 mm (F3) and 1.18-2.36 mm (F2) samples exhibited the minimum strength, and the ratio of various ages to the control group was 86%-88%; the 0.15-0.30 mm (F5) and 0.30-0.60 mm (F4) samples exhibited the maximum strength, and the ratios of the compressive strength at various ages to that of the control group were 96%-98% and 90%-94%. The surface resistance of BOF FA and DSS FA decreased gradually with the 100°C curing age, and fracturing occurred at

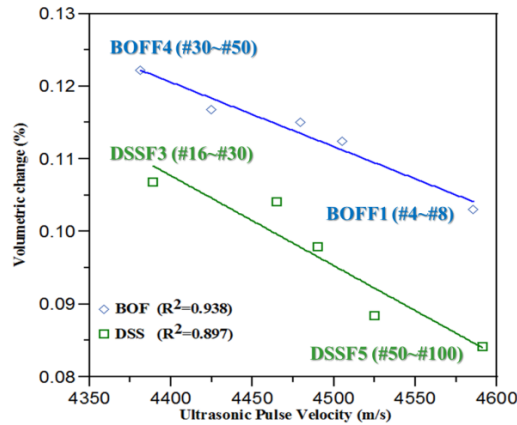


Fig. 11 Slag replaced single particle size volumetric change and ultrasonic pulse velocity relationship (100°C, 14 day)

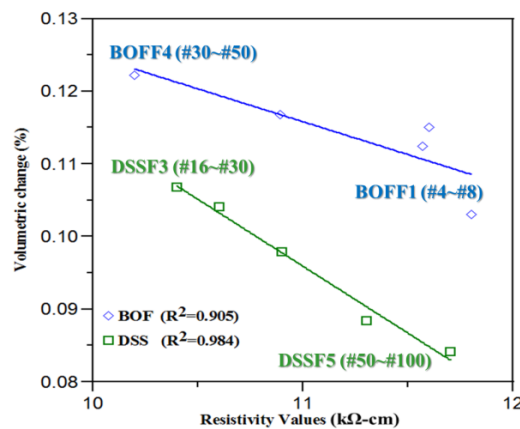


Fig. 12 Slag replaced single particle size volumetric change and resistivity values relationship (100°C, 14 day)

only 5.9 kΩ-cm and 4.3 kΩ-cm, respectively.

The samples deteriorated gradually as the expansion values increased, reducing the compressive strength, ultrasonic pulse velocity, and surface resistance. Figs. 10-12 show the replacement of fine aggregate particles of a single particle size with BOF and DSS on Day 14 of 100°C curing. The compressive strength, ultrasonic pulse velocity, and surface resistance of the mix proportions with the maximum expansion values are lower than those of the other mix proportions, whereas those of the mix proportions with the minimum expansion values are the highest. The R^2 from the regression analysis is greater than 0.9, implying that this relationship is coincident. The expansion reaction of various mix proportions of the complete replacement cured at 100°C was more unstable; thus, the results are lower.

3.4 Scanning electron microscopy (SEM)

After curing of the various mix proportions at 100°C, the main hydration products were CH

and calcium-silicate-hydrate (C-S-H) gel. The CH expanded gradually with the curing age, extruding peripheral hydration products and reducing the C-S-H gel by a relative amount, causing the sample to fracture. On Day 3 of curing, most of the mix proportions contained more C-S-H gel

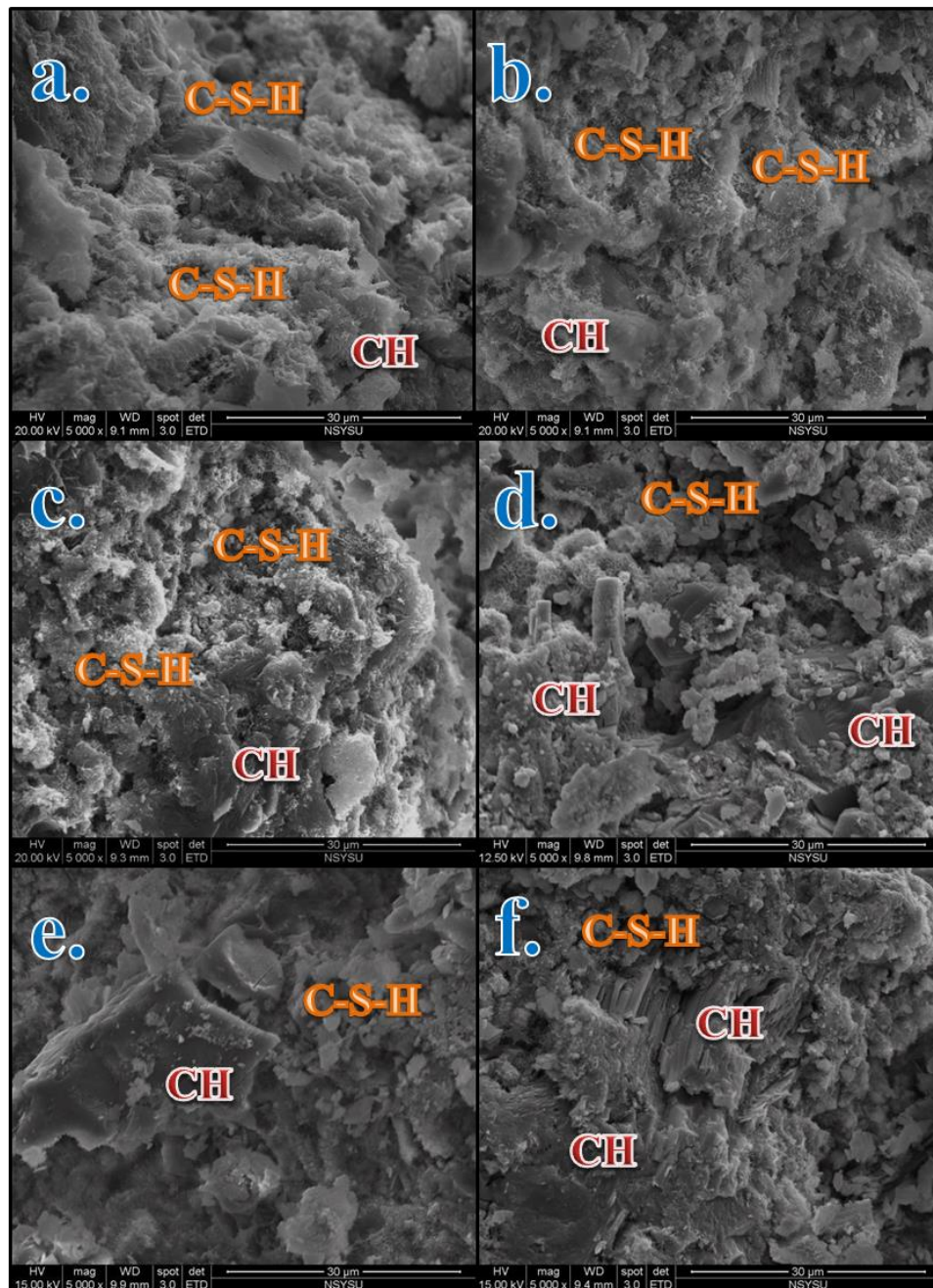


Fig. 13 SEM image analysis BOF concrete ((a)F1; 3 days. (b)F1; 14 days (c)F4; 3 days. (d)F4; 14 days (e)FA; 3 days (f) FA; 5 days) (scales:5000x)

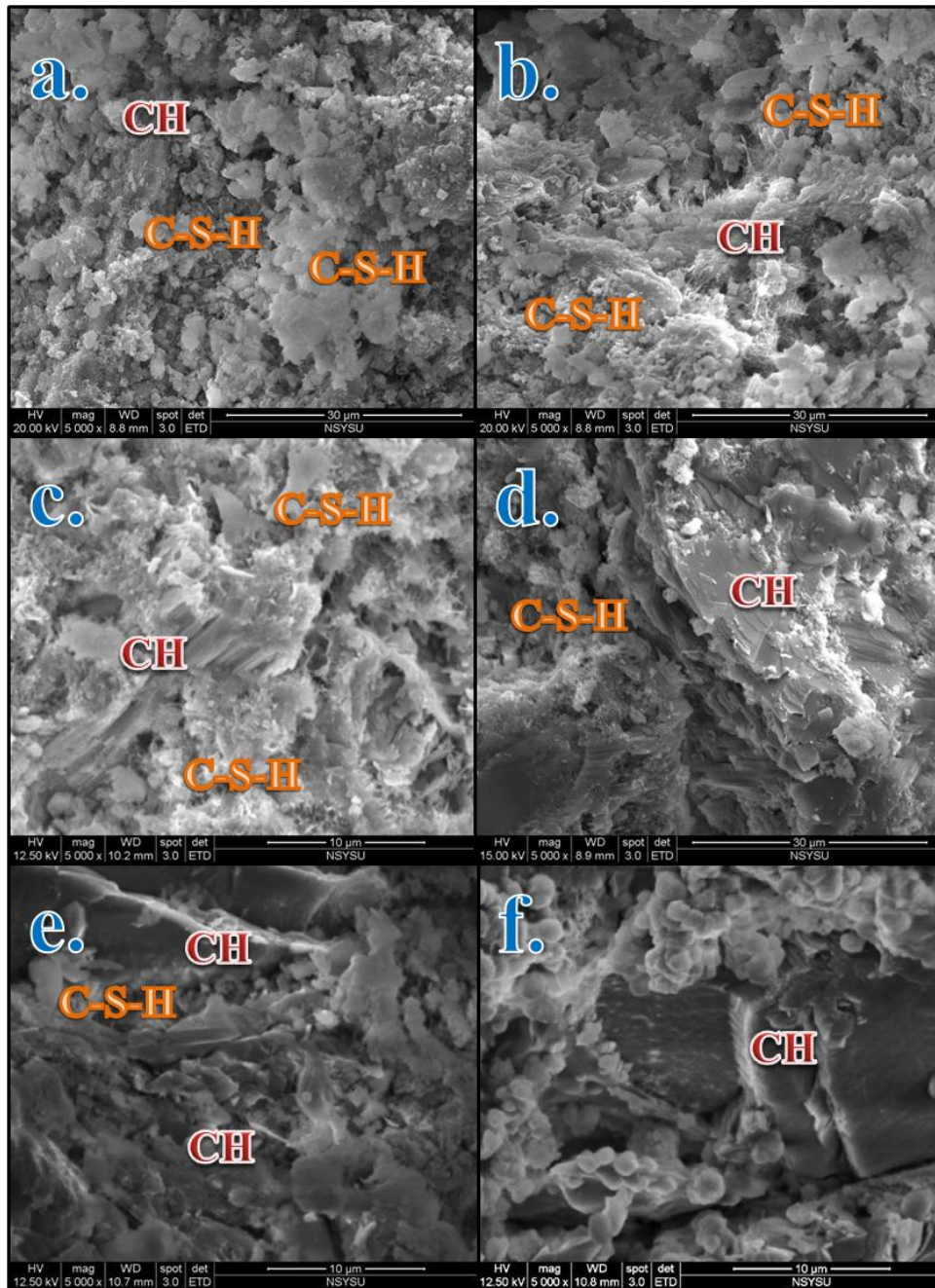


Fig. 14 SEM image analysis DSS concrete ((a)F5;3 days. (b)F5;14 days (c)F3;3 days. (d)F3;14 days (e)FA;3 days (f) FA;11 days) (scales:5000x)

and partial CH, and the mix proportion that expanded unstably contained more CH and C-S-H gel. Regarding the variation of the various mix proportions of BOF with age, the 2.36-4.75 mm (F1) sample exhibited the minimum expansion values. The SEM images on Days 3 and 14 of heat

curing were similar, revealing a large amount of C-S-H gel and partial CH, as shown in Fig. 13(a) and (b). Regarding the 0.30-0.60 mm (F4) sample, which had the maximum expansion values, CH was the major product on Day 14 of curing, and the C-S-H gel was the minor product, as shown in Fig. 13(c) and (d). Fig. 13(e) and (f) shows SEM images of the BOF FA on Day 3 of curing and on the day that the sample fractured (Day 5); because the replacement was higher than the mix proportion of the various groups for replacement of particles of a single size, the CaO content was higher and the hydration process produced additional CH, thereby reducing the amount of C-S-H gel. When the sample fractured, the CH was the major product, and no C-S-H gel was observed. The DSS mix proportion exhibited a slight change in the image of the 0.15-0.30 mm (F5) sample with the minimum expansion values in the curing period, as shown in Fig. 14(a) and (b). In addition, the 0.60-1.18 mm (F3) sample with the maximum expansion values gradually produced CH as the curing time increased, causing the C-S-H gel to become relatively loose, as shown in Fig. 14(c) and (d). The image of the DSS FA on Day 3 of curing differs from that of the mix proportions for the replacement of a single particle size; the CH was the major product, and when the sample fractured (Day 11), the CH was denser and stacked, as shown in Fig. 14(e) and (f).

4. Conclusions

- When particles of a single specific size were replaced with slag and the concrete samples were cured at 100°C, the maximum (F3, F4) and minimum (F1, F5) particle sizes exhibited an expansion effect that was consistent with the autoclave expansion results.
- Replacement of particles 0.30-0.60 mm and 0.60-1.18 mm in size with BOF and DSS, respectively, yielded the greatest expansion.
- After heat curing, the FA concrete samples exhibited severe fractures.
- The compressive strength, ultrasonic pulse velocity, and surface resistance decreased gradually as the expansion values resulting from various mix proportions increased. This was the most noticeable in the mix proportion for complete replacement, which deteriorated rapidly as the expansion reaction intensified, and the sample eventually fractured.
- The SEM results show that the mix proportion for complete replacement produced a considerable amount of CH, which resulted in micro cracking and fracture.
- All aggregate sizes replace more than 25%, there will be expansion of doubt, it is not recommended. And we also must avoid all natural aggregates were replaced with slag aggregates (FA) used in concrete.

Acknowledgements

The authors would like to thank the Ministry of Science and Technology of Taiwan for their financial support of this research under contract No. MOST 103-2221-E-151-047.

References

- Ahmedzade, P. and Sengoz, B. (2009), "Evaluation of steel slag coarse aggregate in hot mix asphalt concrete", *Hazard. Mater.*, **165**(1-3), 300-305.

- Ameri, M. and Ali, B. (2012), "Laboratory studies to investigate the properties of CIR mixes containing steel slag as a substitute for virgin aggregates", *Constr. Build. Mater.*, **26**(1), 475-480.
- ASTM C114, Standard test methods for chemical analysis of hydraulic cement.
- ASTM C1293, Standard test method for determination of length change of concrete due to alkali-silica reaction.
- ASTM C150, Standard specification for portland cement.
- ASTM C151, Standard test method for autoclave expansion of portland cement.
- ASTM C33, Standard specification for concrete aggregates.
- Auriol, J.C. (2004), "Expansion volumique de la chaux et de la magnesia vives (libres) lors de leur hydratation", *Laitiers. Sider.*, **85**, 6-12.
- Bi, C., Zhang, M. and Zhang, Z. (2004), "The application study on CFB slag in concrete", *Fly Ash Comprehensive Utilization*, **4**, 18-20.
- Chaurand, P., Rose, J., Briois, V., Olivi, L., Hazemann, J.L., Proux, O., Domas, J. and Bottero, J.Y. (2007), "Environmental impacts of steel slag reused in road construction: A crystallographic and molecular (XANES) approach", *Hazard. Mater.*, **139**(3), 537-542.
- Cyr, M., Rivard, P. and Labrecque, F. (2009), "Reduction of ASR-expansion using powders ground from various sources of reactive aggregates", *Cement Concrete Compos.*, **31**(7), 436-446.
- Etxeberria, M., Pacheco, C., Meneses, J.M. and Berridi, I. (2010), "Properties of concrete using metallurgical industrial by-products as aggregates", *Constr. Build. Mater.*, **24**, 1594-1600.
- Huang, Y., Bird, R. and Heidrich, O. (2007), "A review of the use of recycled solid waste materials in asphalt pavements", *Resour. Conserv. Recycl.*, **52**(1), 58-73.
- Ivanka, N. (2011), "Utilisation of steel slag as an aggregate in concrete", *Mater. Struct.*, **44**(9), 1565-1575.
- Kamile, T. (2006), "Effect of SO₃ content and fineness on the rate of delayed ettringite formation in heat cured portland cement mortars", *Cement Concrete Compos.*, **28**, 761-772.
- Kelham, S. (2006), "The effect of cement composition and fineness on expansion associated with delayed ettringite formation", *Cement Concrete Compos.*, **18**(3), 171-179.
- Kuo, W.T. and Shu, C.Y. (2014), "Application of high-temperature rapid catalytic technology to forecast the volumetric stability behavior of containing steel slag mixtures", *Constr. Build. Mater.*, **50**, 463-470.
- Kuo, W.T., Shu, C.Y. and Han, Y.W. (2014), "Electric arc furnace oxidizing slag mortar with volume stability for rapid detection", *Constr. Build. Mater.*, **53**, 635-641.
- Kuo, W.T. and Shu, C.Y. (2015), "Expansion behavior of low-strength steel slag mortar during high-temperature catalysis", *Comput. Concrete*, **16**(2), 261-274.
- Li, C.M. and Li, W.J. (2005), "Discussion on quality & expansiveness of expansive material-magnesium oxide", *Des. Hydroelectr. Power Stn.*, **21**(3), 95-99.
- Li, Y.F., Yao, Y. and Wang, L. (2009), "Recycling of industrial waste and performance of steel slag green concrete", *J. Cent. South. Univ. Tech.*, **16**, 768-773.
- Lin, H.Y., Yang, Y.F., Wang, Y.J., Wang, Y.A. and Wang, X.F. (2013), "Effect of aggregate size on ASR expansion and progress of its prediction model", *Bull. Chin. Ceram. Soc.*, **32**(5), 890-894.
- Lin, S.Y. (2006), "Microstructure of expansive BOF slag and its influence on the swelling behaviors", Master Thesis, National Kaohsiung University of Applied Sciences, Taiwan. (in Chinese)
- Lukschova, S., Prikryl, R. and Pertold, Z. (2009), "Petrographic identification of alkali-silica reactive aggregates in concrete from 20th century bridges", *Constr. Build. Mater.*, **23**(2), 734-741.
- Lun, Y., Zhou, M., Cai, X. and Xu, F. (2008), "Methods for improving volume stability of steel slag as fine aggregate", *J. Wuhan. Univ. Technol.*, **3**, 737-742.
- Multon, S., Cyr, M. and Sellier, A. (2010), "Effects of aggregate size and alkali content on ASR expansion", *Cem. Concr. Res.*, **40**(4), 506-516.
- Multon, S., Cyr, M., Sellier, A., Leklou, N. and Petit, L. (2008), "Coupled effects of aggregate size and alkali content on ASR expansion", *Cement Concrete Res.*, **38**(3), 350-359.
- Naganathan, S., Razak, H.A. and Hamid, S.N.A. (2012), "Properties of controlled low-strength material made using industrial waste incineration bottom ash and quarry dust", *Mater. Des.*, **33**, 56-63.
- Naganathan, S., Razak, H.A. and Nadzrian, A.H. (2010), "Effect of kaolin addition on the performance of

- controlled low-strength material using industrial waste incineration bottom ash”, *Waste. Manage. Res.*, **28**(9), 848-860.
- Ortega-Lopez, V., Manso, J.M., Cuesta, I.I. and Gonzalez, J.J. (2014), “The long-term accelerated expansion of various ladle-furnace basic slags and their soil-stabilization applications”, *Constr. Build. Mater.*, **68**, 455-464.
- Poyet, S., Sellier, A., Capra, B., Foray, G., Torrenti, J.M., Cognon, H. and Bourdarot, E. (2007), “Chemical modelling of alkali silica reaction: influence of the reactive aggregate size distribution”, *Mater. Struct.*, **40**(2), 229-239.
- Shen, D.H., Wu, C.M. and Du, J.C. (2009), “Laboratory investigation of basic oxygen furnace slag for substitution of aggregate in porous asphalt mixture”, *Constr. Build. Mater.*, **23**, 453-461.
- Shen, W., Zhou, M., Ma, W., Hu, J. and Cai, Z. (2009), “Investigation on the application steel slag-fly ash-phosphogypsum solidified material as road base material”, *Hazard. Mater.*, **164**(1), 99-104.
- Siddique, R. (2009), “Utilization of waste materials and by-products in producing controlled low-strength materials”, *Resour. Conserv. Recycl.*, **54**(1), 1-8.
- Sofilic, T., Merle, V., Rastovcan-Mioc, A., Cosic, M. and Sofilic, U. (2010), “Steel slag instead natural aggregates in asphalt mixture”, *Arch. Metall. Mater.*, **55**(3), 657-668.
- Sorlini, S., Sanzeni, A. and Rondi, L. (2012), “Reuse of steel slag in bituminous paving mixtures”, *Hazard. Mater.*, **209-210**, 84-91.
- Suer, P., Lindqvist, J.E., Arm, M. and Frogner-Kockum, P. (2009), “Reproducing ten years of road ageing-accelerated carbonation and leaching of EAF steel slag”, *Sci. Total. Environ.*, **407**(18), 5110-5118.
- US federal environment protection agency (2010), Use of recycled industrial materials in roadways. <http://www.epa.gov/osw/conservation/trr/imr/pdfs/roadways.pdf>.
- Waligora, J., Bulteel, D., Degrugilliers, P., Damidot, D., Potdevin, J.L. and Measson, M. (2010), “Chemical and mineralogical characterizations of LD converter steel slags: A multi-analytical techniques approach”, *Mater. Charact.*, **61**(1), 39-48.
- Wang, A., Deng, M., Sun, D., Li, B. and Tang, M.S. (2012), “Effect of crushed air-cooled blast furnace slag on mechanical properties of concrete”, *J. Wuhan. Univ. Technol.-Mater. Sci. Ed.*, **27**(4), 758-762.
- Wang, C.H. (2014), “Feasibility of stabilizing expanding property of furnace slag by autoclave method”, *Constr. Build. Mater.*, **68**, 552-557.
- Wang, G. (2010), “Determination of the expansion force of coarse steel slag aggregate”, *Constr. Build. Mater.*, **24**(10), 1961-1966.
- Wang, G., Wang, Y. and Gao, Z. (2010), “Use of steel slag as a granular material: Volume expansion prediction and usability criteria”, *Hazard. Mater.*, **184**(1-3), 555-560.
- Wu, S., Xue, Y., Ye, Q. and Chen, Y. (2007), “Utilization of steel slag as aggregates for stone mastic asphalt (SMA) mixtures”, *Build. Environ.*, **42**, 2580-2585.
- Yildirim, I.Z. and Prezzi, M. (2009), “Use of steel slag in subgrade applications”, Publication FWA/IN/JTRP-2009/32. Joint Transportation Research Program, West Lafayette, Indiana: Indiana Department of Transportation and Purdue University.
- Yin, L.Q. and Xie, L. (2007), “The application study of circulating fluidized bed boiler slag”, *Elec. Power Environ. Protect.*, **23**(6), 60-62.
- Yu, S.K. (2011), “ASR expansion behavior of recycling waste fine aggregates in concrete”, Master Thesis, National Central University, Taiwan. (in Chinese)